The Journal of Chemical Physics

Mode selective excitation of terahertz vibrations in single crystalline rubrene

Cite as: J. Chem. Phys. **150**, 054503 (2019); https://doi.org/10.1063/1.5068732
Submitted: 18 October 2018 . Accepted: 14 January 2019 . Published Online: 06 February 2019

Keisuke Yano, Hiroyuki Katsuki, and Hisao Yanagi

The Journal of Chemical Physics ARTICLE scitation.org/journal/jcp

Mode selective excitation of terahertz vibrations in single crystalline rubrene

Cite as: J. Chem. Phys. 150, 054503 (2019); doi: 10.1063/1.5068732
Submitted: 18 October 2018 • Accepted: 14 January 2019 •
Published Online: 6 February 2019

Keisuke Yano,[1] Hiroyuki Katsuki,[2,a)] and Hisao Yanagi[2]

AFFILIATIONS

[1]Graduate School of Materials Science, Nara Institute of Science and Technology, 8916-5 Takayama, Ikoma, Nara, Japan
[2]Graduate School of Science and Technology, Nara Institute of Science and Technology, 8916-5 Takayama, Ikoma, Nara, Japan

[a)]Electronic mail: katsuki@ms.naist.jp

ABSTRACT

Organic molecular crystals have a variety of low frequency vibrational modes composed of intra- and inter-molecular oscillations. They are mixed intricately in the terahertz (THz) region. We are interested in the controllability of the vibrational energy distribution among such THz vibrational modes based on the femtosecond double-pulse excitation scheme. Single crystalline rubrene is prepared by physical vapor transport. The optical response of vibrational modes in the electric ground state of rubrene is detected by the ultrafast pump-probe reflectivity measurement at 90 K. Three oscillation modes at 3.20, 3.67, and 4.18 THz are detected, and we demonstrate selective enhancement and depletion of each mode by properly tuning the double-pulse delay. The amplitude of the selected vibrational mode is modulated between 0.149 and 1.87, where 1.0 corresponds to the amplitude excited with a single pump pulse. The double-pulse delay dependence of the observed vibrational amplitude is simulated based on the classical driven harmonic oscillator model, and the results reasonably reproduce our experimental signals. Such selective manipulation of the vibrational amplitude can be a potential tool to investigate the vibronic and electron-phonon couplings which plays an important role for the charge transport characteristics and various optoelectronic properties in organic molecular crystals.

I. INTRODUCTION

Coherent control is a technique to manipulate the properties of a quantum system using the interference of wavefunctions.[1–5] The superposed wavefunctions excited by the time-delayed double pulses show amplitude modulations as we scan the double-pulse delay. We can observe the constructive or destructive overlap of the wavefunctions depending on the double-pulse delay corresponding to the integer or half-integer times the oscillation period of the wave packet motion. Such a kind of coherent control scheme is called wave packet interferometry and has been applied for various kinds of quantum systems, including electronic and vibrational states of gas phase atoms and molecules,[6,7] ro-vibrational states in molecular crystals,[8–10] and excitonic states in semiconductor quantum dots.[11,12] In our previous study, we have manipulated the amplitude of the anti-Stokes scattering signal from the vibrational coherent state of solid *para*-H_2 which is a famous quantum solid known to have extraordinary long vibrational coherence lifetime.[8–10] By superposing vibrational coherent state excited by a pair of time-delayed Raman excitation pulses, we could observe the anti-Stokes radiation whose intensity modulates between 0 and 4 as a function of the double-pulse delay where the signal intensity is normalized to the one pumped by a single excitation pulse.

Another important quantum state which can be controlled in a bulk crystal is the collective motion of optical phonon modes. When the phonon modes are excited impulsively by an ultrashort laser pulse whose temporal width is shorter than the period of phonon oscillation, we can excite collective oscillation of atoms or molecules. Such motion is called coherent optical phonons[13] and have been observed for a variety of solid materials such as bismuth, GaAs, diamonds, and a variety of other semiconductors.[14–24]

Coherent phonons have been intensively studied since the phonon motion reflects the ultrafast deformation of the lattice structure. Various generation mechanisms of the coherent phonons have been discussed[14,15,25] based on the conditions of the excitation laser wavelength, the band structure, and the polarizability of materials. Among them, most popular mechanisms are the displacive excitation of coherent phonons (DECP) and impulsive stimulated Raman scattering (ISRS). For the group of polar semiconductors, transient depletion field screening is also considered as the driving force of coherent phonons.[26] The amplitude control of the coherent phonons has been demonstrated for a crystal of inorganic materials such as bismuth,[18,19,21] YBCO,[22] and diamond[27] using the double-pulse excitation scheme. Assuming the situation that the double pulses are not temporally overlapped with each other, it is reported that the amplitude of the phonon mode is modulated from zero to two as the double-pulse delay is tuned to be half-integer to integer times the phonon oscillation period, where the amplitude is normalized with that of the single pulse excitation.[18] When this technique is applied for a system in which several phonon modes are excited simultaneously, the amplitude distribution can be manipulated since each phonon mode has a different oscillation period.[22] This technique is further developed by utilizing a series of pulse trains and demonstrated as the selective excitation of phonon modes.[28]

In this paper, we apply the double-pulse excitation scheme to the organic single crystal of rubrene to demonstrate the selective excitation and amplitude control of the THz vibrational modes in the electronic ground state. The rubrene has the highest carrier mobility in organic semiconductors and has been applied to various organic devices. The carrier dynamics of rubrene has been studied both electrically and optically.[29–32] The spectroscopic information on the THz vibrational modes in the rubrene crystal has been reported by several groups. In the frequency domain, the polarized Raman spectrum and the temperature dependence of the Raman transition have been reported.[33,34] The assignments of the THz vibrational modes in the ground electronic state have been reported based on the *ab initio* calculations.[33,35] The ultrafast dynamics of energy relaxation in the electronic excited state has been studied mostly related to the interest on the singlet fission process which is related to the vibronic dynamics on the S_1 potential surface.[32,36] Unlike simple inorganic semiconductors and semimetals, the rubrene crystal has a rich spectrum of THz vibrational modes which are the complicated mixture of intra- and inter-molecular vibrational motions. The double-pulse excitation technique is important as a tool to selectively enhance or deplete a THz vibrational mode. Since the modulation of the vibrational amplitude corresponds to the specific modulation of the intra- and inter-molecular motions in the crystal, such a technique can serve as a powerful tool to study the mode-specific vibronic or electron-phonon couplings which may play an important role in the electronic devices.[37–41] One such example has been recently demonstrated by Kim *et al.* for the lead-halide hybrid perovskites.[37] They have performed the THz-pump visible-probe experiment and showed that one typical vibrational mode is strongly coupled to the electronic transitions around the bandgap.

In this paper, we focus on the THz vibrational motions in the electronic ground state using the pump laser photon energy lower than the HOMO-LUMO bandgap. If we utilize laser pulses which is resonant with the electronic absorption, both the DECP and ISRS processes will contribute simultaneously and coherent vibrations are generated both in the electronic excited and ground states. To distinguish the vibrational motions in the ground and excited states, it is important to know the ultrafast vibrational dynamics in the electronic ground state as a starting point. This paper is organized as follows: Sec. II describes the experimental details, Sec. III gives the results of the experiments, and Sec. IV gives the discussion on the experimental results based on the theoretical model. Conclusions are given in Sec. V.

II. EXPERIMENTS

A. Sample preparation

The rubrene crystal has an orthorhombic structure with four rubrene molecules in a unit cell,[42] as shown in Fig. 1(a). Single-crystalline rubrene is prepared by a horizontal physical vapor transport (PVT) method. In our experiment, crystal growth is performed as follows: first, 40 mg of rubrene powder (Sigma-Aldrich, sublimed grade) is placed inside a glass growth tube. The growth tube is purged with nitrogen gas at atmospheric pressure and flowed at a rate of 10 ml/min. The temperature of the glass tube around the source rubrene powder is tuned to keep around 280 °C. The sublimated rubrene molecules are crystalized on the cold wall of the glass tube at the downstream of the flow. As reported in the previous paper,[43] we have obtained re-crystalized rubrene with different morphologies including needle-like, platelet, and other forms of crystals. The platelet crystal is picked up and evaluated by X-ray structural analysis (Rigaku VariMax RAPID RA-Micro7HFM). The orientation of the platelet surface is

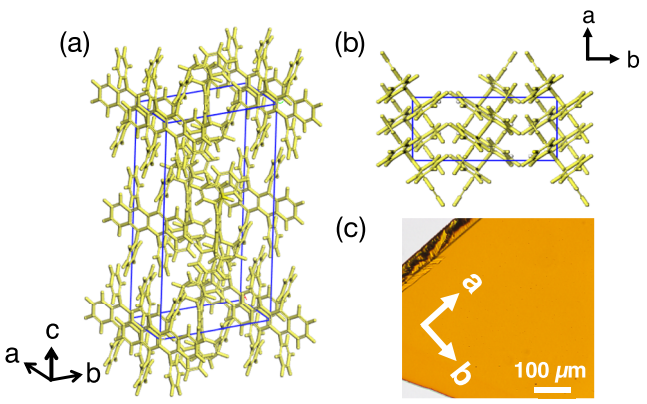

FIG. 1. (a) Crystal structure of rubrene. (b) Molecular packing in the *ab*-plane. (c) A micrograph of a platelet single crystalline rubrene which is prepared by the PVT method.

identified as (001) with the lattice parameter of a = 7.174, b = 14.267, and c = 26.878 Å so that the platelet surface is the ab-plane. The typical ab-plane dimensions are 2 mm × 5 mm. The thickness of the crystal is 10–35 μm. No crack or defect is observed in the microscopic image, as shown in Fig. 1(c). The crystal is placed on a glass plate with a grease, and the glass plate is mounted on a cold copper plate fixed in a liquid nitrogen optical cryostat to be used in the following measurement.

B. Optical setup for transient reflectivity measurement

We have performed the femtosecond (fs) pump-probe measurement to detect the transient reflectivity change ΔR induced by the coherent vibrational excitation. The light source is a mode-locked Ti:sapphire oscillator (Coherent MIRA F-900), providing typically 1.5 W output power with 830 nm central wavelength and the repetition rate of 76 MHz. The temporal full width at half maximum (FWHM) was evaluated with a homemade intensity auto-correlator to be ~110 fs. The fs output pulse is split into pump and probe pulses with 4:1 ratio. The pump pulse is further split into two pulses through the Michelson-type interferometer to generate coaxially aligned time-delayed double pulses. A closed-loop piezo-stage (PI P-621.1CL) is installed in one arm of the interferometer so that we can adjust the relative delay $\Delta\tau$ with sub-femtosecond resolution. The output from the interferometer is focused onto the sample by a plano-convex lens (f = 200). For probing the reflectivity change, we have applied the balanced detection technique to enhance the sensitivity. The probe pulse is split by another beam-splitter, and one part is monitored by using a Si diode photodetector (PD1) as a reference. The remaining part goes through a fast scan unit (APE Scandelay 15) and is focused onto the target sample by a plano-convex lens (f = 120). The polarization of both the pump and probe pulses is set parallel to the b-axis of the rubrene crystal. We did not perform anisotropic reflectivity measurement such as electro-optic sampling so that the main contributions for our coherent vibrational signal are expected to be from symmetric A_g modes. The fast scan unit can sweep the pump-probe delay τ_{pr} over ~15 ps at a repetition rate of 20 Hz. The reflected probe pulse is detected by another Si diode photodetector (PD2). The intensity at each photodetector is adjusted with a variable density filter so that the differential signal from PD1 and PD2 is balanced when the pump pulse does not shine the sample. The differential signal is bandpass-filtered between 3 and 300 kHz, and then amplified with a current amplifier (SRS SR-570) with 200 nA/V gain factor. The impulsive electronic response which arises when the pump and probe pulses are temporally overlapped with each other and the slowly decaying non-oscillatory response are removed through this process. The temperature of the rubrene crystal is set at 90 K during the measurement. The input laser fluence of the single pump pulse and the probe pulse is ~2.2 and ~0.91 μJ/cm^2, respectively. The detected signal is averaged for 512 acquisitions on the oscilloscope to give single scan data, and such scans are further averaged over 30 times on the desktop personal computer.

III. RESULTS

A. Single pulse measurement

Figure 2(a) shows the signal of coherent vibrations in a single-crystalline rubrene excited by a single pump pulse. The time-dependent change of reflectivity $\Delta R/R$ is plotted as a function of pump-probe delay. The slowly modulating baseline is fitted with a 7th order polynomial function and subtracted for further analysis. The sharp peak around τ_{pr}~0 ps is due to the remaining instantaneous electronic response. The inset of Fig. 2(a) shows the oscillatory part of the reflectivity change from τ_{pr} = 0.3 to 6.0 ps after subtracting the slowly varying background signal. To prepare these data, the original data are interpolated to evenly spaced data which are necessary for the following Fourier-transform analysis. Hereafter, we will discuss on this oscillatory part of the observed signal. The complex beating structure indicates the contribution of several vibrational modes. The Fourier-transform of the inset of Fig. 2(a) is plotted in Fig. 2(b). The pump photon energy of 1.49 eV is much smaller than the HOMO-LUMO bandgap energy of 2.32 eV[44] so that direct excitation of the electronic excited state is not taken into account. In the rubrene crystal, the two photon absorption of around 1.49 eV photon is also reported.[45] Under current experimental conditions, however, such a two photon absorption process is negligibly small so that we can safely assume that the coherent vibrations are generated in the electronic ground state by the ISRS scheme. In this case, only the Raman active modes are expected to be detected. Comparing with the former Raman scattering measurement,[33] we can identify three peaks at ~3.20, 3.67, and 4.18 THz, which we call ν_1, ν_2, and ν_3 modes, respectively. Their oscillation periods are calculated to be ~312, 272, and 239 fs, which are hereafter defined as T_1,

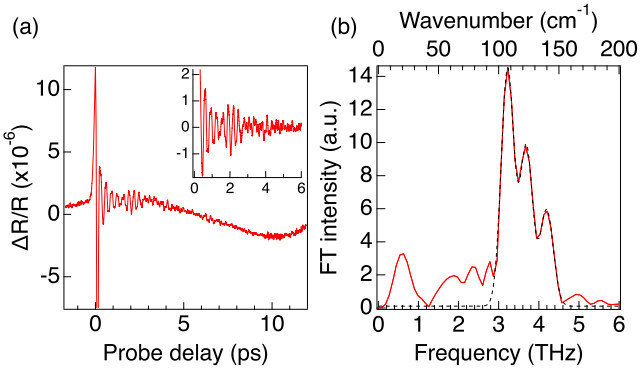

FIG. 2. (a) Observed coherent vibrational signal in rubrene excited by a single pump pulse. The inset is the enlarged oscillatory part of the signal which is interpolated to be evenly spaced after subtraction of the slowly varying baseline. (b) Fourier-transformed spectrum of the THz vibrations calculated from the data in the inset of (a). The black dashed line is the fitted curve based on the three mode model given in Eq. (1).

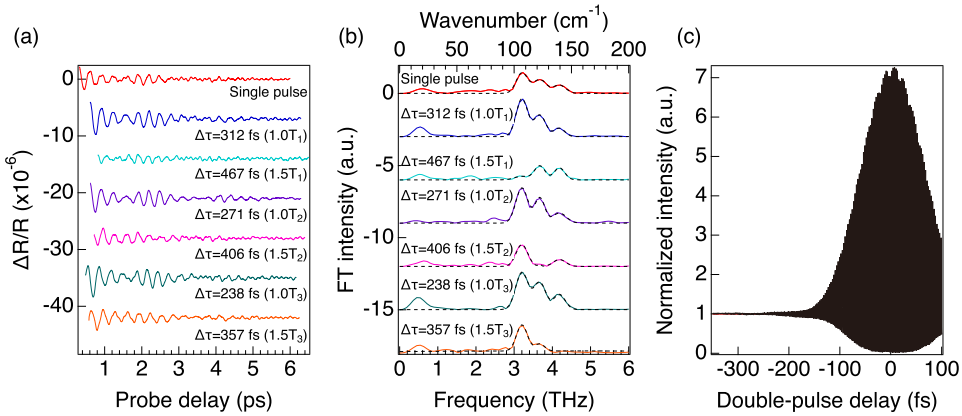

FIG. 3. (a) Observed coherent vibrational signals in rubrene excited by the double pulses. Plots with $\Delta\tau$ = 312, 271, and 238 fs correspond to the constructive timings of ν_1, ν_2, and ν_3 vibrational modes, respectively. Plots with $\Delta\tau$ = 467, 406, and 357 fs correspond to the destructive timings of the same vibrational modes. (b) Fourier-transformed spectra of the THz vibrational signals given in (a). The black dashed lines are the fitted curves based on the three mode model given in Eq. (1). In (a) and (b), the traces other than the single pulse excitation are vertically shifted for clarity. (c) Fringe-resolved interferometric autocorrelation of the excitation double pulses. The influence of the temporal overlap of the double pulses at $|\Delta\tau| > 200$ fs is negligibly small.

T_2, and T_3, respectively. It is known that THz intra- and intermolecular vibrational motions are mixed up intricately in the rubrene crystal.[33,46] According to the previous *ab initio* calculations, these peaks are assigned mainly to the intramolecular vibrational motions. The mixing ratio of the intermolecular phonon motion in ν_1, ν_2, and ν_3 modes is estimated to be 5.9%, 14.6%, and 1.5%, respectively.[33] Based on the temperature dependent Raman spectrum, a crystal temperature lower than 70 K would be necessary to observe the principally intermolecular phonon modes.[34] In Fig. 2(b), there is a low frequency peak around 0.5 THz whose oscillation period corresponds to 2 ps. We cannot find any corresponding Raman peak in the preceding research.[33,34] We will discuss on this peak in Sec. III B. The Fourier-transformed THz spectrum of the coherent vibrational signal can be fitted using a model function

$$g(\nu) = Y_0 + \sum_{i=1}^{3} A_i \exp\left(-\left(\frac{\nu - \nu_i}{\delta_i}\right)^2\right), \quad (1)$$

where Y_0 is the baseline offset and we have included the three vibrational modes with their frequency ν_i, amplitude A_i, and linewidth δ_i {i = 1, 2, or 3}, respectively. The fitted result is plotted in Fig. 2(b) with a black broken line. The discrepancy is rather small so that it is assured that the current three-mode model reasonably reproduces the observed oscillatory signals.

B. Double-pulse measurement

We have applied the double-pulse excitation scheme to demonstrate the manipulation of the vibrational amplitude distribution among the ν_1–ν_3 modes identified in the single pulse measurement. The delay $\Delta\tau$ is tuned to 1.0 and 1.5 times the oscillation period of each vibrational mode, T_1, T_2, and T_3, respectively. Figure 3(a) shows the observed transient reflectivity change after subtracting the baseline, as we have done in the single pulse experiment. Due to the huge non-resonant electronic response which appears around τ_{pr}~0 and ~$\Delta\tau$, we have shown only the oscillatory part after the second pump pulse in Fig. 3(a). In the data shown in Fig. 3(a), the delay $\Delta\tau$ is tuned to be ~1.0T_1 (312 fs), 1.5T_1 (467 fs), 1.0T_2 (271 fs), 1.5T_2 (406 fs), 1.0T_3 (238 fs), and 1.5T_3 (357 fs). The fringe-resolved interferometric autocorrelation of the double pulses shown in Fig. 3(c) assures that the double pulses

TABLE I. Amplitude multiplication factor for each vibrational mode derived from the Fourier-transformed THz spectrum at various intervals of the double pulses.

ν_1		ν_2		ν_3	
Period	Amplitude	Period	Amplitude	Period	Amplitude
Single pulse	1.00	Single pulse	1.00	Single pulse	1.00
1.0T_1	1.87	1.0T_2	1.84	1.0T_3	1.84
1.5T_1	0.171	1.5T_2	0.149	1.5T_3	0.251
2.0T_1	1.78	...	...	...	...
2.5T_1	0.0966	...	...	...	...
3.0T_1	1.59	...	...	...	...

are not temporally overlapped even at the shortest delay of $\Delta\tau$~1.0T_3.

The Fourier-transform of each trace shown in Fig. 3(a) is plotted in Fig. 3(b). When the delay $\Delta\tau$ is tuned to ~1.0T_1 and 1.5T_1, we can observe the enhancement and depletion of the ν_1 mode intensity, as shown in Fig. 3(b). Similarly, the ν_2 and ν_3 mode intensities are enhanced at $\Delta\tau$~1.0T_2 and 1.0T_3 and depleted at $\Delta\tau$~1.5T_2 and 1.5T_3, respectively. The Fourier-transformed spectrum plotted in Fig. 3(b) for each trace is fitted with Eq. (1) and overlapped in Fig. 3(b) with a dashed line. We have used common parameters ν_i and δ_i of each vibrational mode which are fixed to the average values derived from the individual fitting process for all the measured data shown in Fig. 3(b). The only exception is the value of ν_3 at $\Delta\tau$~1.5T_3, which seems to be poorly converged due to the low signal intensity of the ν_3 mode at this timing. The Fourier-transformed intensity of each vibrational mode is compared with that of the single pulse excitation. As shown in Table I, we have performed amplitude multiplication by ~1.85 at the constructive and by ~0.190 at the destructive timing for each of the vibrational modes. This result indicates that highly selective amplitude manipulation can be realized by the simple double-pulse excitation scheme. Concerning the peak around 0.5 THz, similar modulation of the amplitude at different $\Delta\tau$ is observed as shown in Fig. 3(b). Since the frequency of 0.5 THz corresponds to the oscillation period of 2 ps, we should observe a monotonous decrease of the peak amplitude from $\Delta\tau$ = 238 to 467 fs if this peak is originated from molecular vibration. From the data shown in Fig. 3(b), we cannot observe such correlation. Thus we consider that this 0.5 THz peak may be an artifact, for example, due to the systematic calibration error of the fast scan unit.

Figures 4(a) and 4(b) show the coherent vibrational signals and their Fourier-transformed spectra with the delay $\Delta\tau$ tuned to ~1.0T_1 (312 fs), 1.5T_1 (467 fs), 2.0T_1 (623 fs), 2.5T_1 (778 fs), and 3.0T_1 (934 fs). The dashed lines are the fitted results of the Fourier-transformed spectra using Eq. (1) with the same ν_i and δ_i parameters used for the analysis shown in Fig. 3(b). The amplitudes of ν_1 mode at $\Delta\tau$~2.0T_1 to 3.0T_1 are evaluated compared to the single pulse excitation, and the results are listed in Table I.

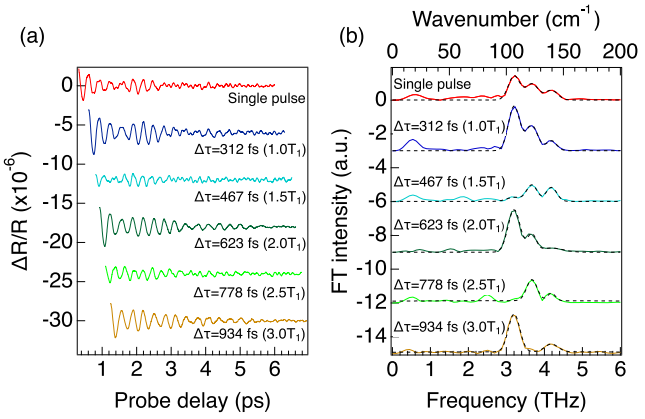

FIG. 4. (a) Coherent vibrational signals and (b) their Fourier-transformed spectra excited by various double-pulse delays from 1.0T_1 to 3.0T_1. The data shown at the top in each panel are the reference signal taken with a single pump pulse. The black dashed lines are the fitted curves based on the three mode model given in Eq. (1). The traces other than the reference are vertically shifted for clarity.

IV. DISCUSSION

Concerning the mechanism of the coherent vibrational excitation in our current experiment, we can safely assume the ISRS mechanism since the photon energy of the laser pulse is much less than the HOMO-LUMO bandgap energy of rubrene. For the measurement of the oscillatory part of the reflectivity change with parallel pump and probe pulses, the relation between the atomic displacement due to the normal mode of vibration and the reflectivity change $\Delta R/R$ is given by[19,47,48]

$$\frac{\Delta R}{R} \propto \sum_i \frac{\partial R}{\partial \chi}\frac{\partial \chi}{\partial q_i} q_i(t), \tag{2}$$

where χ and $q_i(t)$ are the diagonal part of the susceptibility tensor and atomic displacement of mode ν_i, respectively. From this equation, we can assume that the reflectivity change is proportional to the atomic displacement. The equation of motion for $q_i(t)$ can be described by the driven harmonic oscillator model given as[13]

$$\frac{d^2 q_i}{dt^2} + 2\gamma_i \frac{dq_i}{dt} + \omega_i^2 q_i = \frac{F_i(t)}{M_i}, \tag{3}$$

where γ_i is the damping factor, ω_i is the angular frequency, M_i is the effective mass, and $F_i(t)$ is the external force applied by the pump pulse for the vibrational mode ν_i. The external force $F_i(t)$ under the ISRS scheme is given as[49]

$$F_i(t) = \frac{1}{2}\left(\frac{\partial \chi}{\partial q_i}\right)_0 |\mathbf{E}(t)|^2. \tag{4}$$

Within this model, we obtain the vibrational amplitude which is proportional to the intensity of the electric field. Assuming that the first pump pulse arrives at t = 0, the Gaussian-shaped electric field envelope of the double pulses is written as

$$\mathbf{E}(t) = \hat{\mathbf{b}} E_0 \left[e^{-4\ln 2\left(\frac{t}{\tau_p}\right)^2} + e^{-4\ln 2\left(\frac{t-\Delta\tau}{\tau_p}\right)^2} \right], \tag{5}$$

where τ_p is the FWHM of the electric field of the single pulse, E_0 is the amplitude of the electric field, and $\hat{\mathbf{b}}$ is the unit vector parallel to the b-axis. The parameter E_0 is determined so that the vibrational amplitude immediately after the pump pulse is scaled to unity. Equation (5) is valid when the double pulses are not temporally overlapped with each other. In the following analysis, τ_p is taken to be 156 fs, which corresponds to the experimentally observed intensity FWHM of 110 fs. Using Eqs. (3)–(5), we can simulate the coherent vibrational signal excited by the double pulses. For simplicity, we focus on the behavior of the specific vibrational mode, ν_1, in the following analysis. Examples of the reflectivity change simulated at $\Delta\tau$ = 2.0T_1 and 1.5T_1 are plotted in Figs. 5(a) and 5(b), respectively. Here we use the vibrational frequency $\omega_1/2\pi$ = 3.20

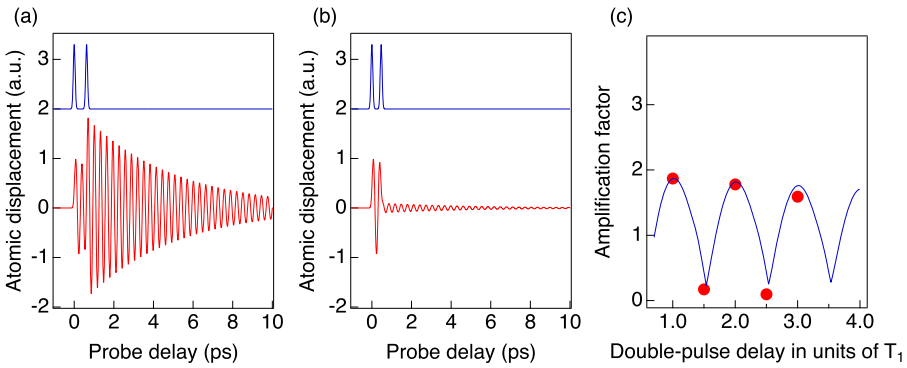

FIG. 5. (a) and (b) Calculated atomic displacement based on the driven harmonic oscillator model. The red curve is the atomic displacement for ν_1 mode, and the blue curve is the intensity profile of the pump pulse. The double-pulse delay is set to (a) $2.0T_1$ and (b) $1.5T_1$, respectively. (c) (Red dots) Amplitude of the ν_1 vibrational modes derived from the intensity spectrum shown in Fig. 4(b). (Blue curve) Simulated vibrational amplitude estimated from the maximum amplitude after the second pulse irradiation.

THz and the damping factor γ_1 = 4.46 which are derived from the fitting parameters of Eq. (1) used for Fig. 3(b). Figure 5(c) shows the simulated ν_1 mode amplitude at different double-pulse delays $\Delta\tau$ together with the experimental results listed in Table I. The abscissa is the multiplication factor n defined as $\Delta\tau = nT_1$. The vibrational amplitude is defined in the same manner, as given in Figs. 5(a) and 5(b). When the double pulses are no longer temporally overlapped, the cancellation and enhancement of the amplitude occur periodically as $\Delta\tau$ comes near the half-integer or integer times T_1. Such amplitude modulation between 0 and 2 has been reported in the previous experiment for inorganic crystals.[18,27] The slow decrease of the contrast at longer time scale is simply due to the decay of the vibrational amplitude prepared by the first pump pulse. Here we have shown only the simulation result for ν_1 mode, but it can be applied straightforwardly for other modes.

We have demonstrated the high-contrast vibrational mode annihilation in Fig. 3(b). In the above experiments, the selective excitation of a single vibrational mode is not achieved since the timing of the maximum amplitude enhancement of one mode is not exactly the timing of depletion for other modes. If we tune the delay $\Delta\tau$ to a longer value, more flexible manipulation of the vibrational population distribution is possible. For example, the delay $\Delta\tau$ of 2.99 ps corresponds to $9.58T_1$, $11.03T_2$, and $12.56T_3$. Thus we can selectively excite ν_2 mode and almost deplete ν_1 and ν_3 modes, if we tune $\Delta\tau$ to this timing. It is also possible to enhance the mode selectivity if we utilize a pulse train with equal intervals which is tuned to an integer multiple of the T_i period, as demonstrated by Weiner *et al.*[28] The different THz spectra shown in Fig. 3(b) represent that we can design the structure of the heat bath composed of THz intra- and inter-molecular vibrational modes. In the future experiment, the vibronic and electron-phonon couplings will be investigated under the designed population distribution among the intra- and inter-molecular vibrations, tuning the pump photon energy resonant to the electronic transitions.

V. CONCLUSION

In conclusion, we have demonstrated the selective amplification of coherent THz vibrational motion in a single crystalline rubrene by using the time-delayed double-pulse excitation scheme. By tuning the double-pulse delay to integer or half-integer times the specific vibrational period, we can enhance or deplete the amplitude of the vibrational mode between ~1.87 and ~0.149 times compared to the single pulse excitation. The results are well reproduced by a simulation based on the driven harmonic oscillator model. This technique will help us to prepare a simplified testbed to study the vibronic and electron-phonon couplings where one specific vibrational mode is efficiently coupled with the electron dynamics in complex organic crystals.

ACKNOWLEDGMENTS

The authors gratefully acknowledge Mr. S. Katao (Nara Institute of Science and Technology) for helping the X-ray diffraction measurements. This work was supported by JSPS KAKENHI (Grant Nos. 26287093 and 18H01900).

REFERENCES

[1] P. Brumer and M. Shapiro, Chem. Phys. Lett. **126**, 541 (1986).
[2] D. J. Tannor and S. A. Rice, J. Chem. Phys. **83**, 5013 (1985).
[3] T. C. Weinacht, J. Ahn, and P. H. Bucksbaum, Nature **397**, 233 (1999).
[4] T. Brixner, G. Krampert, T. Pfeifer, R. Selle, G. Gerber, M. Wollenhaupt, O. Graefe, C. Horn, D. Liese, and T. Baumert, Phys. Rev. Lett. **92**, 208301 (2004).
[5] M. P. A. Branderhorst, P. Londero, P. Wasylczyk, C. Brif, R. L. Kosut, H. Rabitz, and I. A. Walmsley, Science **320**, 638 (2008).
[6] N. F. Scherer, R. J. Carlson, A. Matro, M. Du, A. J. Ruggiero, V. R. Rochin, J. A. Cina, G. R. Fleming, and S. A. Rice, J. Chem. Phys. **95**, 1487 (1991).
[7] E. W. Lerch, X. Dai, S. Gilb, E. A. Torres, and S. R. Leone, J. Chem. Phys. **124**, 044306 (2006).
[8] H. Katsuki, Y. Kayanuma, and K. Ohmori, Phys. Rev. B **88**, 014507 (2013).
[9] H. Katsuki, K. Ohmori, T. Horie, H. Yanagi, and K. Ohmori, Phys. Rev. B **92**, 094511 (2015).
[10] H. Katsuki and K. Ohmori, J. Chem. Phys. **145**, 124316 (2016).
[11] T. Suzuki, R. Singh, M. Bayer, A. Ludwig, A. D. Wieck, and S. T. Cundiff, Phys. Rev. Lett. **117**, 157402 (2016).
[12] N. H. Bonadeo, J. Erland, D. Gammon, D. Park, D. S. Katzer, and D. G. Steel, Science **282**, 1473 (1998).
[13] R. Merlin, Solid State Commun. **102**, 207 (1997).
[14] W. A. Kutt, W. Albrecht, and H. Kurz, IEEE J. Quantum Electron. **28**, 2434 (1992).
[15] K. J. Yee, Y. S. Lim, T. Dekorsy, and D. S. Kim, Phys. Rev. Lett. **86**, 1630 (2001).

[16]G. C. Cho, W. Kütt, and H. Kurz, Phys. Rev. Lett. **65**, 764 (1990).
[17]K. Ishioka, M. Kitajima, and O. V. Misochko, J. Appl. Phys. **103**, 123505 (2008).
[18]M. Hase, K. Mizoguchi, H. Harima, S. Nakashima, M. Tani, K. Sakai, and M. Hangyo, Appl. Phys. Lett. **69**, 2474 (1996).
[19]M. F. DeCamp, D. A. Reis, P. H. Bucksbaum, and R. Merlin, Phys. Rev. B **64**, 092301 (2001).
[20]A. V. Bragas, C. Aku-Leh, S. Costantino, A. Ingale, J. Zhao, and R. Merlin, Phys. Rev. B **69**, 205306 (2004).
[21]H. Katsuki, J. C. Delagnes, K. Hosaka, K. Ishioka, H. Chiba, E. S. Zijlstra, M. E. Garcia, H. Takahashi, K. Watanabe, M. Kitajima, Y. Matsumoto, K. G. Nakamura, and K. Ohmori, Nat. Commun. **4**, 2801 (2013).
[22]Y. Okano, H. Katsuki, Y. Nakagawa, H. Takahashi, K. G. Nakamura, and K. Ohmori, Faraday Discuss. **153**, 375 (2011).
[23]H. Wang, L. Valkunas, T. Cao, L. Whittaker-Brooks, and G. R. Fleming, J. Phys. Chem. Lett. **7**, 3284 (2016).
[24]W. Albrecht, Th. Kruse, and H. Kurz, Phys. Rev. Lett. **69**, 1451 (1992).
[25]A. V. Kuznetsov and C. J. Stanton, Phys. Rev. B **51**, 7555 (1995).
[26]M. Först and T. Dekorsy, "Coherent phonons in bulk and low-dimensional semiconductors," in *Coherent Vibrational Dynamics*, edited by S. De Silvestri, G. Cerullo, and G. Lanzani (CRC, Boca Raton, 2008), pp. 129–172.
[27]H. Sasaki, R. Tanaka, Y. Okano, F. Minami, Y. Kayanuma, Y. Shikano, and K. G. Nakamura, Sci. Rep. **8**, 9609 (2018).
[28]A. M. Weiner, D. E. Leaird, G. P. Wiederrecht, and K. A. Nelson, J. Opt. Soc. Am. B **8**, 1264 (1991).
[29]A. L. Briseno, R. J. Tseng, M.-M. Ling, E. H. L. Falcao, Y. Yang, F. Wudl, and Z. Bao, Adv. Mat. **18**, 2320 (2006).
[30]A. Saeki, S. Seki, T. Takenobu, Y. Iwasa, and S. Tagawa, Adv. Mat. **20**, 920 (2008).
[31]V. C. Sundar, J. Zaumseil, V. Podzorov, E. Menard, R. L. Willett, T. Someya, M. E. Gershenson, and J. A. Rogers, Science **303**, 1644 (2004).
[32]K. Miyata, Y. Kurashige, K. Watanabe, T. Sugimoto, S. Takahashi, S. Tanaka, J. Takeya, T. Yanai, and Y. Matsumoto, Nat. Chem. **9**, 983 (2017).
[33]E. Venuti, I. Bilotti, R. G. D. Valle, and A. Brillante, J. Phys. Chem. C **112**, 17416 (2008).
[34]Z. Q. Ren, L. E. McNeil, S. Liu, and C. Kloc, Phys. Rev. B **80**, 245211 (2009).
[35]J. R. Weinberg-Wolf, L. E. McNeil, S. Liu, and C. Kloc, J. Phys.: Condens. Matter **19**, 276204 (2007).
[36]B. A. West, J. M. Womick, L. E. McNeil, K. J. Tan, and A. M. Moran, J. Phys. Chem. C **114**, 10580 (2010).
[37]H. Kim, J. Hunger, E. Cánovas, M. Karakus, Z. Mics, M. Grechko, D. Turchinovich, S. H. Parekh, and M. Bonn, Nat. Commun. **8**, 687 (2017).
[38]G. Batignani, G. Fumero, A. R. S. Kandada, G. Cerullo, M. Gandini, C. Ferrante, A. Petrozza, and T. Scopigno, Nat. Commun. **9**, 1971 (2018).
[39]A. A. Bakulin, R. Lovrincic, X. Yu, O. Selig, H. J. Bakker, Y. L. A. Rezus, P. K. Nayak, A. Fonari, V. Coropceanu, J.-L. Brédas, and D. Cahen, Nat. Commun. **6**, 7880 (2015).
[40]M. Hada, K. Norimatsu, S. Tanaka, S. Keskin, T. Tsuruta, K. Igarashi, T. Ishikawa, Y. Kayanuma, R. J. D. Miller, K. Onda, T. Sasagawa, S. Koshihara, and K. G. Nakamura, J. Chem. Phys. **145**, 024504 (2016).
[41]A. K. Basak, H. Petek, K. Ishioka, E. M. Thatcher, and C. J. Stanton, Phys. Rev. B **91**, 125201 (2015).
[42]D. E. Henn, W. G. Williams, and D. J. Gibbons, J. Appl. Cryst. **4**, 256 (1971).
[43]A. R. Ullah, A. P. Micolich, J. W. Cochrane, and A. R. Hamilton, Proc. SPIE **6800**, 680005 (2007).
[44]O. Mitrofanov, D. V. Lang, C. Kloc, J. M. Wikberg, T. Siegrist, W.-Y. So, M. A. Sergent, and A. P. Ramirez, Phys. Rev. Lett. **97**, 166601 (2006).
[45]P. Irkhin and I. Biaggio, Phys. Rev. B **89**, 201202(R) (2014).
[46]P. Ordejón, D. Boskovic, M. Panhans, and F. Ortmann, Phys. Rev. B **96**, 035202 (2017).
[47]T. E. Stevens, J. Kuhl, and R. Merlin, Phys. Rev. B **65**, 144304 (2002).
[48]T. Garl, E. G. Gamaly, D. Boschetto, A. V. Rode, B. Luther-Davies, and A. Rousse, Phys. Rev. B **78**, 134302 (2008).
[49]G. A. Garrett, T. F. Albrecht, J. F. Whitaker, and R. Merlin, Phys. Rev. Lett. **77**, 3661 (1996).